KECK Geology Consortium
Learning Science Through Research
Published by the Keck Geology Consortium
Short Contributions
Keck Geology Consortium
Volume 33
May 2020

PRE-ERUPTIVE TEMPERATURES AND ERUPTION DYNAMICS OF RHYOLITE LAVA, NIMBIN RHYOLITE, EASTERN AUSTRALIA

CHLOE CAMPO, Trinity University
Research Advisor: Kurt Knesel

INTRODUCTION

Although the emplacement of aerially extensive rhyolitic lava is less well understood compared to mafic lavas, the geological record shows that rhyolites typically form thicker, shorter flows compared to their mafic counterparts (Walker, 1973). This observation is consistent with the strong influence of viscosity on lava emplacement (Huppert, 1982). In order to better understand the influence of pre-eruptive temperature and magma composition on the viscosity and emplacement of aerially extensive rhyolitic lavas, I analyzed the compositions of phenocrysts, microphenocrysts, and matrix glass in obsidian from the Nimbin Rhyolite, eastern Australia.

The Nimbin Rhyolite is a complex of coalescing rhyolite lava domes and flows on the southwestern flank of the Tweed shield volcano (Duggan and Mason, 1978). Individual lavas are comprised of flow-banded rhyolite varying in thickness from 50 to 150 m and have spread up to 5 km from their respective vents (Ewart et al. 1987; Smith and Houston, 1995). Flow bands in the glassy portions of the lavas are composed of alternating bands of brown and colorless glass. The lavas range from nearly aphyric to up to about 30 vol. % crystals, comprised of quartz, sanidine, plagioclase, orthopyroxene, clinopyroxene and ilmenite.

METHODS

Scanning Electron Microscopy

Energy-dispersive analysis (EDS) was used to characterize the chemistry of glass, phenocrysts, and microphenocrysts using the JEOL JSM-6010LA SEM at Trinity University. Operating conditions included an accelerating voltage of 20 kV, count times of 30 seconds, working distance of 10 mm, a count rate of approximately 10,000 cps and ZAF correction method. Standard measurements for augite (NMNH-133868, Kakanui, New Zealand), anorthite (NMNH-137041, Great Sitkin Island, Ak), anorthoclase (NMNH-133868, Kakanui, New Zealand), and basalt glass (NMNH-111240-52, Juan de Fuca Ridge) were taken to evaluate the accuracy and precision of the EDS measurements. Mean values, along with the standard deviations, for replicate analyses of each standard are presented in Campo (2020). All elements fell within the reference values for their respective standards, with the following exceptions: Al_2O_3 and FeO were about 10% low and 8% high, respectively, in the glass standard, and Al_2O_3 was 7% to 8% low in the feldspar standards. These discrepancies do not influence any of our interpretations. The 2σ uncertainties estimated by replicate standard analysis for elements utilized for geothermometry are 2% for Na_2O (anorthoclase) and CaO (anorthite), 4% for MgO (augite), and 10% for FeO (augite).

Two-Feldspar Thermometry

Two-feldspar thermometry relies on the exchange between albite and anorthite in feldspar, a primarily temperature dependent exchange. Here we use the formulization of Putirka (2008), where temperature (°C) is given by:

$$T = \frac{-442 - 3.72P(kbar)}{-0.11 + 0.11ln(\frac{X_{Ab}^{afs}}{X_{Ab}^{pl}}) - 3.27(X_{An}^{afs}) + 0.098ln(X_{An}^{afs}) + 0.52(X_{An}^{pl}X_{Ab}^{pl})}$$

where XAb^{afs} is the albite content in alkali feldspar, XAb^{pl} is the albite content in plagioclase feldspar, XAn^{afs} is the anorthite content in alkali feldspar, and XAn^{pl} is the anorthite content in plagioclase feldspar. This expression represents a global calibration from 41 experimental observations and maintains an uncertainty of ±30ºC (Putirka, 2008).

Two-Pyroxene Thermometry

Two-pyroxene thermometry relies on the exchange of enstatite and ferrosilite. We employ the recent global regression by Putirka (2008), which yields the following expression:

$$\frac{10^4}{T} = 13.4 - 3.4ln\left(\frac{X^{cpx}_{EnFs}}{X^{opx}_{EnFs}}\right) + 5.59ln\left(X^{cpx}_{Mg}\right) - 8.8\left(Mg\#^{cpx}\right) + 23.85\left(X^{opx}_{Mn}\right) + 6.48\left(X^{opx}_{FmAl_2SiO_6}\right) - 2.38\left(X^{cpx}_{Di}\right) - 0.044P(kbar)$$

where $XEnFs^{cpx}$ is the enstatite content of clinopyroxene, $XEnFs^{opx}$ is the enstatite content of orthopyroxene, XMg^{cpx} is the magnesium content of clinopyroxene, XMn^{opx} is the manganese content of orthopyroxene, $XFmAl_2SiO_6{}^{opx}$ is the $FmAl_2SiO_6$ content of orthopyroxene, and XDi^{cpx} is the diopside content of clinopyroxene. Although this particular model has an uncertainty of ±45ºC (Putirka, 2008), it works best for mafic systems where Mg# of cpx is >0.75. Therefore, because of our inability to employ two-oxide thermometry (given the absence of magnetite), we use the two-pyroxene thermometer as an independent check on *relative* variations in temperature that were identified through feldspar thermometry.

RESULTS

Glass and Mineral Chemistry

Major-element compositions of the glassy flow bands were analyzed along a vertical transect across two thin sections from the Minyon Falls flow of the Nimbin Rhyolite. Forty-two analyses were conducted within 9 brown bands and 59 analyses were made within 8 clear bands. Mean glass values are summarized in Table 1, while the full glass dataset is presented in Camp (2020). The two glass types are remarkably similar in composition. Brown-colored glass bands averaged 77.55 ± 0.50% for SiO_2, 0.99 ± 0.15% for FeO, and 0.60 ± 0.08% for CaO (Table 1). Clear-colored glass bands averaged 77.57 ± 1.14% for SiO_2, 0.98 ± 0.43% for FeO, and 0.56 ± 0.20% for CaO (Table 1). The SEM glass results are consistent with an XRF analysis of a bulk glass separate reported by Duggan (1974); all elemental oxides measured by SEM are, within our estimated 2σ uncertainties, indistinguishable from the XRF results. The same observation holds for the mean (anhydrous) whole-rock values reported in Duggan (1974), which is consistent with the aphyric nature of the Minyon Falls Rhyolite.

The mean compositions of plagioclase, sanidine, and pyroxene analyzed by SEM are summarized in Table 1. The most noteworthy feature is seen between the plagioclase phenocryst and micro-phenocryst populations. Plagioclase phenocrysts vary little in composition and are classified as oligoclase, when oxide components are recast as molecular endmembers. Phenocryst cores have a

Table 1. SEM-EDS analyses of selected phases.

	Brown Glass (35)	σ	Clear Glass (59)	σ	Plagioclase Cores (10)	σ	Plagioclase Rims (6)	σ	Plagioclase Micro-phenocrysts (4)	σ	Sanidine Cores (4)	σ	Pyroxene Cores (9)	σ
Na_2O	2.70	0.26	2.77	0.63	7.46	1.13	7.90	0.34	5.61	0.80	3.64	0.22	0.59	0.46
Al_2O_3	11.67	0.24	11.79	0.67	21.30	1.89	22.03	0.23	25.80	1.14	17.70	0.32	1.91	1.16
SiO_2	77.55	0.50	77.57	1.14	64.62	2.94	63.53	0.38	57.44	1.52	66.51	0.36	51.65	2.20
K_2O	6.01	0.34	5.94	0.73	1.90	0.66	1.67	0.09	0.49	0.28	11.60	0.33	-	-
CaO	0.60	0.08	0.56	0.20	4.77	0.72	4.64	0.42	10.08	1.37	0.44	0.13	1.60	0.19
FeO	0.99	0.15	0.98	0.43	0.19	0.12	0.24	0.12	0.57	0.14	0.12	0.14	33.02	2.30
MgO	0.12	0.08	0.12	0.06	-	-	-	-	-	-	-	-	10.10	1.53
TiO_2	0.17	0.09	0.16	0.07	-	-	-	-	-	-	-	-	0.23	0.16
MnO	0.08	0.07	0.09	0.08	-	-	-	-	-	-	-	-	0.89	0.22
P_2O_5	0.15	0.10	0.15	0.09	-	-	-	-	-	-	-	-	-	-

mean anorthite content of 24 ± 2 mol%, while the mean rim composition is 22 ± 2 mol% (Table 1). Maximum core-to-rim variation is 5.8 mol% An. Although the plagioclase rims and cores appear to be compositionally indistinguishable, they are strikingly distinct from the plagioclase microphenocrysts, which are more calcic with a mean anorthite content of 48 ± 2 mol% (Table 1; Fig. 1). These results are in excellent agreement with available EMPA results. Duggan (1974) reported phenocryst cores and rims with average anorthite contents of 23 ± 3 mol% and and 22 ± 1 mol%, respectively, and groundmass plagioclase with an average anorthite content of 48% ± 2 mol%.

Two-Feldspar Thermometry

Sanidine and plagioclase feldspar compositions from both the SEM data measured here and EMPA data from Duggan (1974) were used for the two-feldspar temperature calculations. To evaluate the influence of pressure on temperatures derived from the thermometer, temperatures were calculated at 10, 50, 100, 150 and 200 MPa. Temperatures increase by less than 10°C per 100 MPa pressure increase. Therefore, for a range of pressures appropriate for magma chambers in the upper crust, the influence of pressure is less than the uncertainty associated with the Putrika (2008) formulization for a single temperature. Using a pressure of 200 MPa, which may be the optimal depth for magma chamber formation (Huber et al., 2019), the plagioclase phenocrysts yield a mean temperature of 810 ± 18ºC, whereas the average temperature for the microphenocrysts is 934 ± 28ºC (Fig. 2).

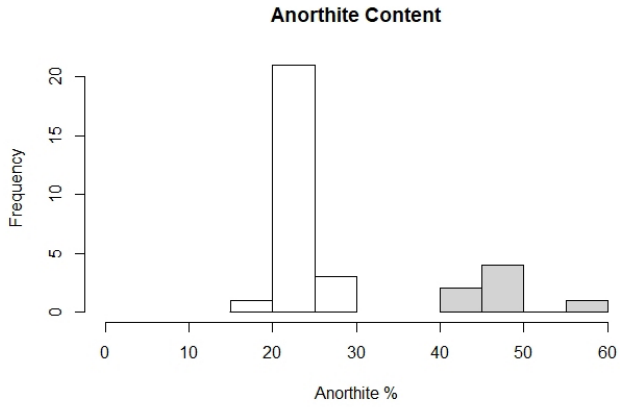

Figure 1. Anorthite content of plagioclase phenocrysts (white) and microphenocrysts (grey).

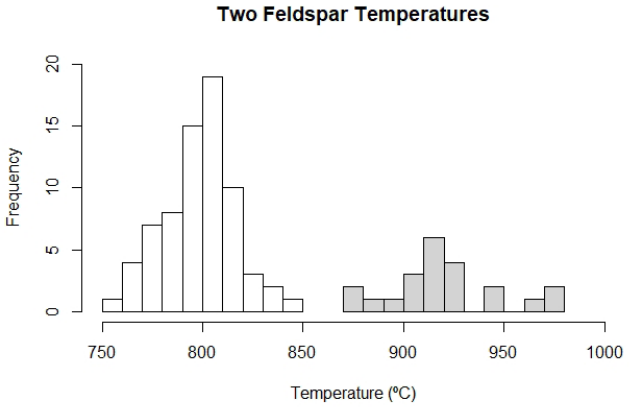

Figure 2. Temperatures calculated using two-feldspar thermometry (Putirka, 2008) for phenocrysts (white) and microphenocrysts (grey).

Two-Pyroxene Thermometry

To further test for relative temperature variations between phenocryst and microphenocryst populations, the limited clinopyroxene and orthopyroxene compositions determined by EMPA (Duggan, 1974) were used in the two-pyroxene thermometer of Putrika (2008). The thermometer shows a similarl (small) dependence on pressure (< 10°C per 100 MPa) to that noted for the two-feldspar thermometer. Using a pressure of 200 MPa, Fe-rich pyroxene phenocrysts yield a mean temperature of 976 ± 85ºC, and Mg-rich groundmass pyroxenes produce a mean temperature of 1101 ± 37ºC.

DISCUSSION

Origin of bimodal mineral chemistry and pre-eruptive temperatures

Chemical analysis by SEM and EMPA show that microphenocrystic and groundmass plagioclase and pyroxene in the Nimbin Rhyolite record heightened values of CaO and MgO compared to their respective phenocrysts. Two-feldspar thermometry indicates the An-rich plagioclase microphenocrysts grew at pre-eruptive temperatures approximately 100ºC hotter than their phenocrystic counterparts (Fig. 2). Similarly, the heightened MgO values in groundmass pyroxenes yield two-pyroxene temperature estimates about 100ºC hotter than lower MgO phenocrysts (Fig. 3). Thus, both thermometers point to a late-stage thermal event in the magma's history. Given the compositionally

bimodal volcanism of the Tweed volcano, this heating event was likely driven by injection of mafic magma. A question remains, however, as to whether the invading magma mixed with the resident magma or simply transferred heat to it.

Magma mixing in silicic magma is often recorded by both bimodal mineral chemistry and distinctive flow banding of contrasting color and major-element composition (Gibson and Naney, 1992; Seaman et al., 1995). However, SEM analysis shows that the clear- and brown-colored glass bands in the Minyon Falls Rhyolite are compositionally indistinguishable (Table 1). Therefore, it appears that neither the flow banding nor the chemical distinction between the phenocrysts and microphenocrysts were the result of mixing of compositionally distinct magmas. This conclusion is consistent with analysis of microlite size and number densities indicating that flow banding in the rhyolite arose from textural heterogeneities developed during shallow magma ascent (Seitzinger and Knesel, 2020; Seitzinger, this volume).

The compositional variations in CaO and MgO between plagioclase and pyroxene phenocrysts and their respective microphenocrysts and the implied late-stage increase in temperature, therefore, appear most likely associated with emplacement of hotter, more mafic magma that did not physically mix with the rhyolitic magma. Such a heating event would lead to resorption of the sodic plagioclase and less mafic pyroxene phenocrysts. This scenario is supported by the generally resorbed nature of the phenocrysts.

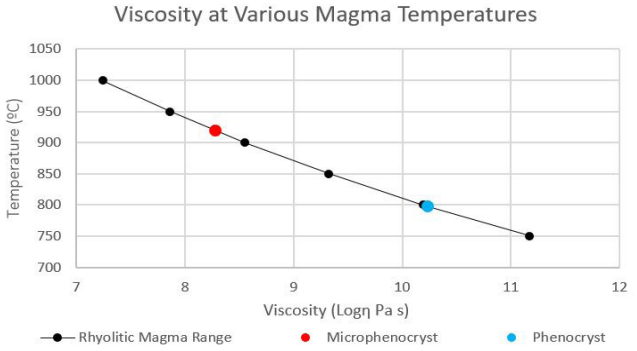

Figure 3. Viscosity of magma as a function of temperature, calculated using the formulization of Giordano et al. (2008). See text for details. The range of temperatures and viscosities for rhyolitic magma is shown in black. The blue dot represents the viscosity calculated based on the average plagioclase phenocryst temperature; the red dot represents the viscosity calculated for the average plagioclase microphenocryst temperature.

In contrast, the microphenocrysts display a range of acicular, swallowtail, and skeletal textures, indicating they likely crystallized rapidly during magma ascent (Kirkpatrick et al., 1979; Swanson et al., 1989).

Implications for lava emplacement

In order to explore the impact that pre-eruptive heating may have on magma rheology and the flow of lava at the surface, we first utilized a Vogel-Fulcher-Tammann (VFT) equation for temperature dependence on viscosity (Giordano et al., 2008). The viscosity η is given by

$$log\eta = A + \frac{B}{T(K) - C}$$

where parameter A is a constant, parameters B and C are linear ensembles of combinations of the oxide components, and T is the temperature of the magma in Kelvin. The constant A represents a high-temperature limit to silicate melt viscosity, taken as -4.55 ± 0.21 (Giordano et al., 2008). Parameters B and C are calculated based on mol. % oxides from the melt composition, with B representing 10 coefficients and C representing 7 coefficients (Giordano et al., 2008). Using a water content of 0.13 wt % H_2O, representative of highly degassed rhyolite (Friedman et al., 1963; Liu et al., 2005), and a melt composition obtained from the mean for whole-rock XRF analyses reported in Duggan (1974), the resulting viscosities for the mean two-feldspar microphenocryst and phenocryst temperatures are $10^{8.18}$ Pa s and $10^{10.12}$ Pa s, respectively (Fig. 3). These calculations show that an increase in temperature of about 100°C produces a decrease in viscosity of roughly two orders of magnitude.

Finally, to investigate how these variations in viscosity may have impacted the emplacement of rhyolite, we calculated the distance R that lava flows from the vent using the equation (Huppert et al., 1982)

$$R = 0.7\left(\frac{\rho g V^3}{3\eta}\right)^{1/8} t^{1/8}$$

where ρ is the density (kgm^{-3}), η is the viscosity (Pa s), V is the eruptive volume (m^3), g is 9.8 ms^{-2}, and t is time (s). Due to lack of constraint on lava

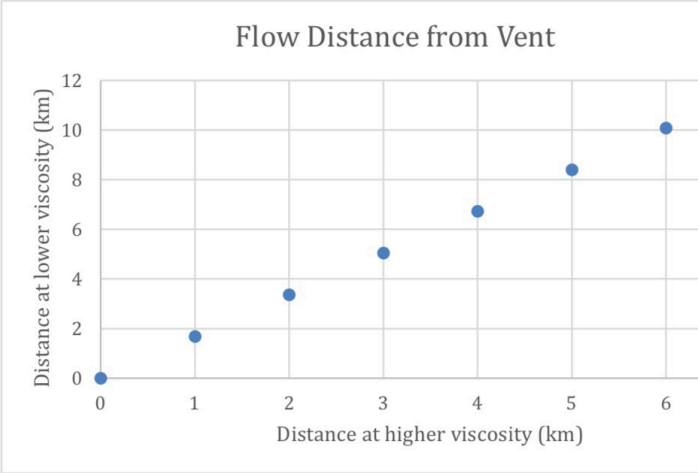

Figure 4. Impact of the temperature-dependent reduction in magma viscosity shown in Figure 3 on lava flow distance. X-axis represents baseline flow distance (R) from vent, with no reduction in magma viscosity. Y-axis represents flow distances augmented by a temperature increase of 100°C and resulting decrease in viscosity of ~100 Pa s, arising from the relationship $R \alpha \eta^{-1/8}$ *(Huppert, 1982). See text for details.*

emplacement time, we used the relative relationship between viscosity and distance ($R \alpha \eta^{-1/8}$), which yields an ~68% increase in flow distance for the lower viscosity calculated from the microphenocryst two-feldspar temperatures (Fig. 4). The apparent reduction in viscosity associated with late-stage heating may have added up to 2 km to the length of rhyolite lavas of the Nimbin dome complex, which extend up to 5 km from their respective vents.

CONCLUSIONS

Rhyolite flows of the Nimbin dome complex preserve information regarding a pre-eruptive thermal event in which underplating facilitated the eruption and subsequent aerially extensive emplacement of rhyolitic lava. An increase in CaO and MgO in plagioclase and pyroxene microphenocrysts compared to their respective phenocrysts points to the heating event, while chemical homogeneity of colorless and brown-colored flow bands eliminates the possibility of magma mixing or mingling. Magma underplating is commonplace in the geologic record and the Nimbin dome complex is one example that illustrates the potential importance of thermal rejuvenation and consequent reduction in viscosity for the emplacement of rhyolitic lava.

ACKNOWLEDGEMENTS

This material is based upon work supported by the Keck Geology Consortium and the National Science Foundation under Grant no. 1659322. Special thanks to my advisor, Dr. Kurt Knesel, for his unwavering guidance and patience throughout this project. I am also grateful to Dr. Jennifer Steele for her help in training and guidance with the SEM and to Dr. Diane Smith for access to her SEM standards. Thank you to my fellow Keck Geology Consortium researchers, Brooke Dykstra, Juli Flint, and Zenja Seitzinger, for a great experience in the field.

REFERENCES

Campo, C. (2020) Pre-eruptive temperatures and eruption dynamics of rhyolite lava, Nimbin Rhyolite dome complex, eastern Australia. Senior Thesis, Trinity University.

Duggan, M. B. (1974) The Mineralogy and Petrology of the Southern Portion of the Tweed Shield Volcano, Northeastern New South Wales. PhD Thesis, University of New England, Armidale.

Duggan, M. B., and Mason, D. R. (1978) Stratigraphy of the Lamington Volcanics in far northeastern New South Wales. Journal of the Geological Society of Australia, 25, 65-73.

Ewart, A, Stevens, N. C., and Ross, J. A. (1987) The Tweed and Focal Peak shield volcanoes, southeastern Queensland and northeastern New South Wales. Papers of the Department of Geology University of Queensland, 11, 1-82.

Friedman, I., Long, W., and Smith, R. L. (1963) Viscosity and water content of rhyolite glass. Journal of Geophysical Research, 68 (24), 6523–6535, doi:10.1029/JZ068i024p06523.

Gibson, R.G. and Naney, M.T., 1992, Textural development of mixed, finely porphyritic silicic volcanic rocks, Inyo Domes, eastern California. Journal of Geophysical Research, 97, 4541–4559.

Giordano, D., Russell, James K., Dingwell, Donald B. (2008) Viscosity of magmatic liquids: A model. Earth and Planetary Science Letters, 271, 123-134, doi:10.1016/j.epsl.2008.03.038.

Huber, C., Townsend, M., Degruyter, W., and Bachmann, O. (2019) Optimal depth of

subvolcanic magma chamber growth controlled by volatiles and crust rheology. Nature Geoscience, 12, 762-768. 10.1038/s41561-019-0415-6.

Huppert, H.E., Shepherd, J.B., Sigurdsson, H., Sparks, R.S.J. (1982) On lava dome growth, with application to the 1979 lava extrusion of the Soufriere of St. Vincent. Journal of Volcanology and Geothermal Research, 14, 199–222.

Kirkpatrick, R. J., Klein, L., Uhlmann, D. R., and Hays, J. F. (1979) Rates and processes of crystal growth in the system anorthite-albite. Journal of Geophysical Research, 84, 3671-3676.

Liu, Y., Zhang, Y., and Behrens, H. (2005) Solubility of H2O in rhyolitic melts at low pressures and a new empirical model for mixed H2O-CO2 solubility in rhyolitic melts. Journal of Volcanology and Geothermal Research, 143, 219-235.

Putirka, Keith D. (2008) Thermometers and Barometers for Volcanic Systems. Reviews in Mineralogy and Geochemistry, 69, 61-120, doi: 10.2138/rmg.2008.69.3.

Seaman, S. J., Scherer, E. E., & Standish, J. (1995) Multistage magma mingling and the origin of flow banding in the Aliso lava dome, Tumacacori Mountains, southern Arizona. Journal of Geophysical Research, 100(B5), 8381-8398. https://doi.org/10.1029/94JB03260.

Seitzinger, Z., and Knesel, K. (2020) Flow bands and microlite textures in obsidian, Minyon Falls Rhyolite, Australia. Geological Society of America Abstracts with Programs, 52, No. 5, doi: 10.1130/abs/2020NC-348340.

Smith, J.V., and Houston, E.C. (1995) Structure of lava flows of the Nimbin Rhyolite, northeast New South Wales. Australian Journal of Earth Sciences, 42, 69-74, doi: 10.1080/08120099508728179.

Swanson, S. E., Naney, M. T., Westrich, H. R., Eichelberger, J. C. (1989) Crystallization history of Obsidian Dome, Inyo Domes, California. Bulletin of Volcanology, 51, 161-176.

Walker, G. P. L. (1973) Lengths of lava flows. Phil Trans R Soc London A 274, 107–118.